

Annual Review of Physical Chemistry

Atomic Force Microscopy: An Emerging Tool in Measuring the Phase State and Surface Tension of Individual Aerosol Particles

Hansol D. Lee and Alexei V. Tivanski

Department of Chemistry, University of Iowa, Iowa City, Iowa 52242, USA; email: hansol-lee@uiowa.edu, alexei-tivanski@uiowa.edu

Annu. Rev. Phys. Chem. 2021. 72:235-52

First published as a Review in Advance on January 11, 2021

The Annual Review of Physical Chemistry is online at physchem.annualreviews.org

https://doi.org/10.1146/annurev-physchem-090419-

Copyright © 2021 by Annual Reviews. All rights reserved

ANNUAL CONNECT

www.annualreviews.org

- Download figures
- Navigate cited references
- Keyword search
- · Explore related articles
- Share via email or social media

Keywords

single particle, hygroscopicity, phase state, surface tension, atomic force microscopy, aerosols

Abstract

Atmospheric aerosols are suspended particulate matter of varying composition, size, and mixing state. Challenges remain in understanding the impact of aerosols on the climate, atmosphere, and human health. The effect of aerosols depends on their physicochemical properties, such as their hygroscopicity, phase state, and surface tension. These properties are dynamic with respect to the highly variable relative humidity and temperature of the atmosphere. Thus, experimental approaches that permit the measurement of these dynamic properties are required. Such measurements also need to be performed on individual, submicrometer-, and supermicrometer-sized aerosol particles, as individual atmospheric particles from the same source can exhibit great variability in their form and function. In this context, this review focuses on the recent emergence of atomic force microscopy as an experimental tool in physical, analytical, and atmospheric chemistry that enables such measurements. Remaining challenges are noted and suggestions for future studies are offered.

1. INTRODUCTION

Atmospheric aerosol particles are suspended particulate matter of varying composition, size, mixing state, and phase state (1, 2). Primary sources of aerosols include the burning of fossil fuels, mineral dust, volcanic eruptions, and sea spray. Sea spray aerosols (SSAs) in particular are composed of complex organic, inorganic, and biological mixtures that originate from the ocean surface and are emitted to the atmosphere via bubble bursting (3, 4). Secondary sources emit aerosols that undergo heterogeneous chemical reactions with volatile precursors in the atmosphere, with secondary organic aerosols (SOAs) being one of the most common examples (5, 6). Primary and secondary aerosols exist in both sub- and supermicrometer sizes and have a significant impact on the climate, atmosphere, and human health (1). For example, fine particulate matter (e.g., PM_{2.5}) can travel through the respiratory system and into the alveolar region of the lungs, leading to cardiovascular and respiratory diseases (7). Atmospheric aerosols can help to regulate the climate either directly by scattering and reflecting solar radiation (8) or indirectly by nucleating clouds as cloud condensation nuclei (CCN) or ice nucleating particles (INPs) (9-11). However, significant uncertainties hinder our ability to accurately assess the direct and indirect effects of aerosols on the climate (12). A significant source of this uncertainty originates from the dynamic nature of the atmospherically relevant physicochemical properties of aerosols, as they vary greatly with changing environmental conditions, e.g., relative humidity (RH) and temperature. These properties must be elucidated using both ensemble-averaging and single-particle techniques, as the effect of changing environmental conditions varies on individual particles, which then affects certain physicochemical properties such as hygroscopicity (the propensity of an aerosol to take up water) (13-17), phase state (5, 13, 15, 18-26), and surface tension (27-31). Therefore, instrumentation and corresponding methodologies need to be developed to measure these aerosol properties.

Toward this end, atomic force microscopy (AFM) has become an emerging tool for the study of both submicrometer- and supermicrometer-sized aerosols. AFM experiments can be performed either under vacuum or in ambient pressure conditions as well as in liquid media (32-35). AFM uses a sharp probe or tip, as sharp as 1 nm in tip radius of curvature, to obtain a sample image by raster scanning a surface via direct contact, intermittent contact/tapping/AC, or noncontact imaging modes (32). Images based on the sample height, vertical piezo position, AFM tip amplitude, phase, deflection, and other factors can be obtained with nanometer-level spatial resolution (36-41). Once located, particles deposited on a substrate (in this case) can be studied using contact mode force spectroscopy. The same AFM imaging tip can be used to measure forces acting on the tip as a function of tip-sample separation during vertical tip movement toward and away from the sample surface (38). The resultant so-called force plots can be obtained with controlled scan rate, maximum applied force, and overall distance while varying the RH and temperature. The force plots pertain directly to several important physicochemical properties of the system studied. This single-particle methodology has previously been applied to directly measure the phase state and surface tension of SSA-relevant model systems (42-45) and real SSAs (4, 46, 47). The mixing state and hygroscopicity have also been measured with AFM via the AC imaging mode while varying the RH (4, 47–50).

AFM, similar to other techniques that are covered in this review (except for the particle rebound method), is an offline technique. The aerosols first need to be collected on a solid substrate and then transferred onto the microscope for measurements. The substrate is typically an inert, clean surface (e.g., silicon, gold, silver, mica, or glass) where the particles of interest are deposited. Depending on the type of study, hydrophobically coated substrates may be used (43). Deposition is commonly performed using an impactor that deposits the stream of particles onto multiple impaction plates that exclude the aerosols based on aerodynamic size (50). One advantage to studying

substrate-collected particles is that the sample can be revisited multiple times after the deposition. However, one disadvantage is that the impaction may modify the original morphology of suspended aerosols (50). Additionally, sample storage conditions must be appropriate to ensure that sample aging and/or handling does not alter the particles of interest (51). AFM, along with some other techniques, can analyze the data on an individual particle-to-particle basis, which can reveal important and unique outliers to the population data set that may otherwise go undetected. For aerosol types such as SSAs that exhibit unique specificity, where only 1 in 10^6 become INPs at -25° C (52, 53), single-particle sensitivity is imperative to further elucidate the role of aerosols in the climate and atmosphere.

So far, single-particle AFM has seen increasing use to study SSA-relevant model systems and real SSAs by directly measuring their hygroscopicity, phase state, and surface tension on a single-particle basis. In the following sections, the role of hygroscopicity in aerosol-climate interactions and how it affects the phase state, viscosity, and surface tension of aerosols are discussed. Here, we also demonstrate that hygroscopicity is an example of the importance of using single-particle techniques. Then, AFM methodology to measure the phase state and surface tension of aerosols is reviewed in the context of other existing techniques as they apply toward both ensemble-averaging and bulk and single-particle studies. Finally, this review concludes by noting the challenges that remain as well as suggestions for future studies.

2. HYGROSCOPICITY OF AEROSOLS AFFECTS THEIR PHASE STATE, VISCOSITY, AND SURFACE TENSION

Depending on the RH and temperature, aerosols that contain water-soluble chemical components tend to take up more water (i.e., be more hygroscopic) than do those that contain more insoluble components (14). Additionally, some aerosol types such as SSAs exhibit a complex mixing of both water-soluble and insoluble components (4, 54). As hygroscopicity strongly depends on the chemical composition and mixing state of the aerosol, measuring it directly is important. Finally, because the amount of water absorbed by the aerosol changes the solute concentration (55), it further modulates the solute concentration–dependent physicochemical properties such as viscosity, phase state, and surface tension (28, 30, 43, 56, 57). Therefore, we begin with a discussion of aerosol hygroscopicity and its role in the dynamics of the aerosol–climate relationship.

First, hygroscopicity is important because it can modulate the viscosity and phase state of the aerosol by altering its solute concentration as a function of RH. Depending on the hygroscopicity of an aerosol, a variable RH environment yields different solute concentrations, which changes its viscosity and phase state. In the atmosphere, solid-like particles behave differently than do liquid-like particles; the solids (viscosity $>10^{12}$ Pa·s) or semisolids (viscosity range 10^2-10^{12} Pa·s) exhibit significantly lower diffusion coefficients than do the liquids (viscosity $<10^2$ Pa·s), which leads to a relatively low reactivity with atmospheric gases (22, 24), an increased tendency for ice nucleation through heterogeneous freezing (15, 58, 59), and the suppression of water uptake (26, 60, 61).

Second, hygroscopicity controls the size of aerosols at a particular RH, which affects their light-scattering efficiency via the direct aerosol effect (17, 62). Finally, hygroscopicity is one of the variables required to determine the efficiency of the aerosol to become a cloud droplet, which grows into a cloud as CCN. For example, hygroscopicity of the aerosol is taken into account in the κ -Köhler theory (10),

$$\frac{\rm RH}{100} = \frac{D_{\rm w}^3 - D_{\rm d}^3}{D_{\rm w}^3 - D_{\rm d}^3(1 - \kappa)} \exp\left(\frac{4\sigma M_{\rm w}}{RT \rho_{\rm w} D_{\rm w}}\right),$$
1.

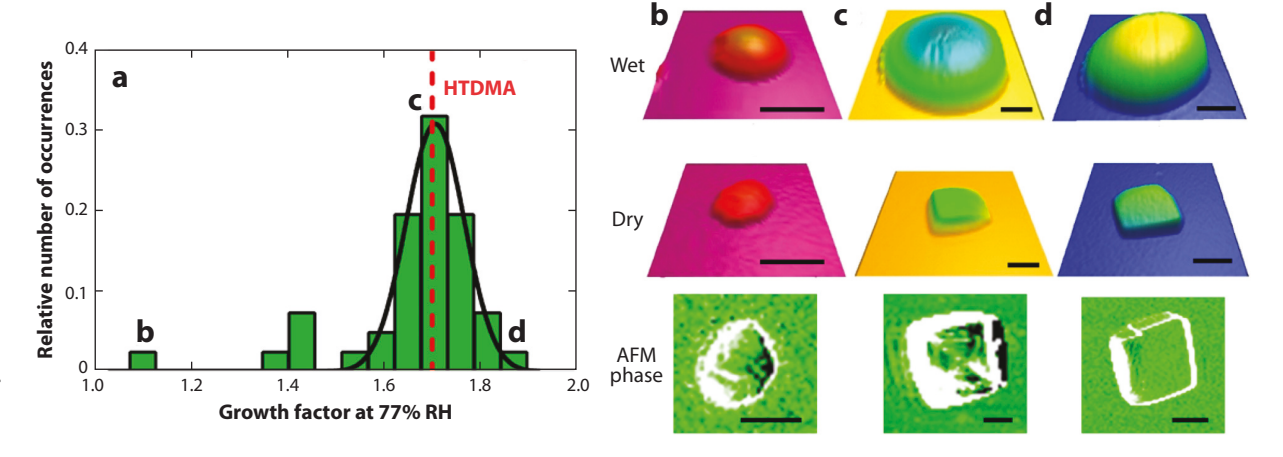


Figure 1

(a) Graph showing a comparison of growth factor measurements at 77% RH for AFM (green bars) versus HTDMA (red dashed vertical line) of a 6:1 molar NaCl:nonanoic acid mixture. The solid black line is a Gaussian fit. (b-d) Three-dimensional AFM height images of individual particles shown in panel a from (middle row) dry to (top row) wet states. (Bottom row) AFM phase images of dry individual particles. Scale bars represent 500 nm. Abbreviations: AFM, atomic force microscopy; HTDMA, hygroscopic tandem differential mobility analyzer; RH, relative humidity. Figure adapted with permission from Reference 49; copyright 2016 American Chemical Society.

where $D_{\rm w}$ is the wet diameter, $D_{\rm d}$ is the dry diameter, κ is a hygroscopicity parameter, σ is the surface tension of the aerosol, $M_{\rm w}$ is the molecular weight of water, R is a gas constant, and $\rho_{\rm w}$ is the density of water. The hygroscopicity parameter κ and the extent of the difference between the wet and dry diameters refer to how hygroscopic the aerosol is. For example, both a high hygroscopicity parameter value and a large difference between the wet and dry diameters indicate a greater propensity for water uptake by the aerosol, which leads to decreases in the solute concentration as the relative amount of water increases. Soluble species such as inorganic salts typically have higher hygroscopicity parameter values than do insoluble organic species such as long-chain fatty acids (10, 63, 64).

Furthermore, the importance of single-particle studies is illustrated by evaluating the hygroscopic nature of multicomponent aerosols that exhibit a diverse range of chemical mixing ratios. As shown in **Figure 1**, single-particle AFM height imaging and a hygroscopic tandem differential mobility analyzer (HTDMA) were used to measure the hygroscopic growth factor (GF) of a 6:1 molar ratio of NaCl:nonanoic acid, which was aerosolized from a bulk solution (49). GF is defined as

$$GF = \frac{D_{\rm w}}{D_{\rm d}}$$
 2.

and can be used as an indicator of hygroscopicity. The data show that while the average of the AFM GF data correlates well with that of the HTDMA, the latter is unable to observe the uniquely different hygroscopic responses of individual aerosols within the population. This illustrates the importance of single-particle capabilities to complement the existing bulk or ensemble-averaging techniques.

In the following sections, we discuss how the viscosity, phase state, and surface tension of aerosols are measured for sub- and supermicrometer particles.

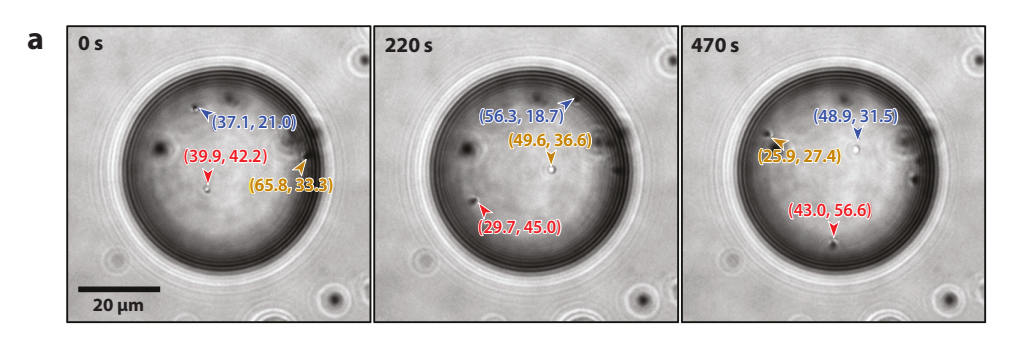
3. VISCOSITY AND PHASE STATE MEASUREMENTS OF AEROSOLS

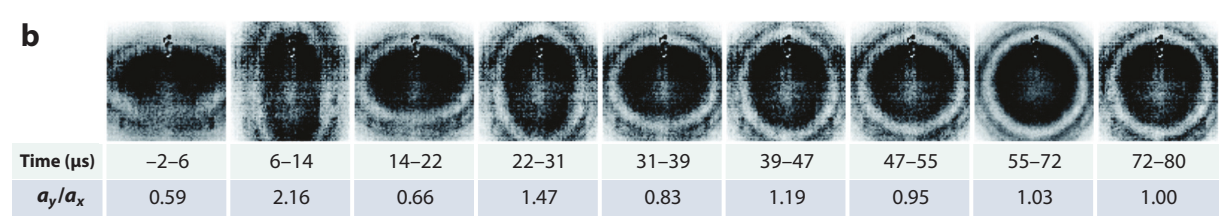
Typically, the viscosity of bulk liquids is measured using viscometers (65), which are well established, inexpensive, and easy to use. However, they require a minimum volume of liquid, and the methods are constrained to quantifying viscosities below 10⁸ Pa·s (66). Therefore, other techniques are needed to measure the viscosity and phase state of aerosols. In fact, it is desirable for these other techniques to be able to measure the viscosities of aerosols up to 10¹⁶ Pa·s. By and large, this topic has been reviewed previously for various techniques that can probe organic aerosols (66). However, AFM capabilities were not mentioned. We therefore briefly review other existing techniques before discussing the AFM methodology in detail.

Several techniques can quantify the viscosity and phase state of aerosols (**Figure 2**). The first is the bead-mobility technique (**Figure 2***a*) (21, 67, 68), which works by injecting 1- μ m-sized melamine beads into 30–50- μ m-sized particles on a substrate. A gas is flowed over the particle surface to circulate the beads, and the velocity of the beads is measured using optical microscopy to infer the viscosity from 10⁻³ to 10³ Pa·s. The second technique is optical tweezers (**Figure 2***b*) (56, 57, 66, 69, 70). This technique works by trapping two supermicrometer aerosols, coalescing them into a single aerosol, and quantifying the relaxation time. The relaxation time is directly proportional to the aerosols' viscosity, which can be quantified from 10⁻³ to 10⁹ Pa·s. The third is the poke-and-flow technique (**Figure 2***c*) (21, 71). It works by locating a supermicrometer-sized particle on a substrate with optical microscopy, indenting the particle surface with a needle, and observing the time taken to reestablish the equilibrium shape. The resulting data are compared with the theoretical flow time to infer the aerosol viscosity from 10³ to 10⁷ Pa·s.

The aforementioned techniques can measure the viscosity and infer the phase state of aerosols. But techniques also exist that can identify the phase state without measuring the viscosity. Particle rebound is one such technique (Figure 3) (72–74). It relies on using an impaction device to separate the aerosol particles by size and deposit both sub- and supermicrometer particles onto substrates. Upon impaction, solid-like particles tend to bounce off more from the substrate, whereas liquid-like particles tend to adhere to the surface. The rebound factor, which is defined as the fraction of particles that bounced, is measured on model systems, and data from nascent aerosols are compared against the model systems to infer the phase state. While some suggest that this methodology is applicable only from 100 to 102 Pa·s, other studies show that it can be extended to as high as 106 Pa·s (74). Microfluidics is another technique that can identify the aerosol phase state (75–77). Individual supermicrometer droplets can be generated and trapped within microfluidic channels that are filled with a lubricating liquid (e.g., silicone oil). Trapped droplets begin to dehydrate, as the surrounding environment is less humid, and the resultant phase transitions are captured by an inverted optical microscope (76). In addition to observing phase transitions from liquid to solid phases, more complex mixing states such as liquid-liquid phase separation can also be observed by this technique (75, 78).

AFM can be used to directly identify the phase state of individual substrate-deposited particles as a function of RH. Specifically, by utilizing AFM force spectroscopy, force plots that contain measured force versus tip–sample separation data are collected for individual particles at a selected position and a specific RH (**Figure 4**). Here, a decrease in the tip–sample separation corresponds to the AFM tip vertically approaching the particle surface. Prior to contact with the particle, at around zero tip–sample separation, long-range attractive interactions between the tip and the particle surface contribute to a further lowering of the tip position. Upon contact, the tip continues its downward trajectory and indents into the particle (negative tip–sample separation) until the measured force increases to a predefined force value. Afterward, the probe retracts until the tip and particle are no longer in contact. The force plots over the same particle are repeatedly collected at varying RHs, in either hydration or dehydration mode (42, 44, 46). For the phase state assessment,





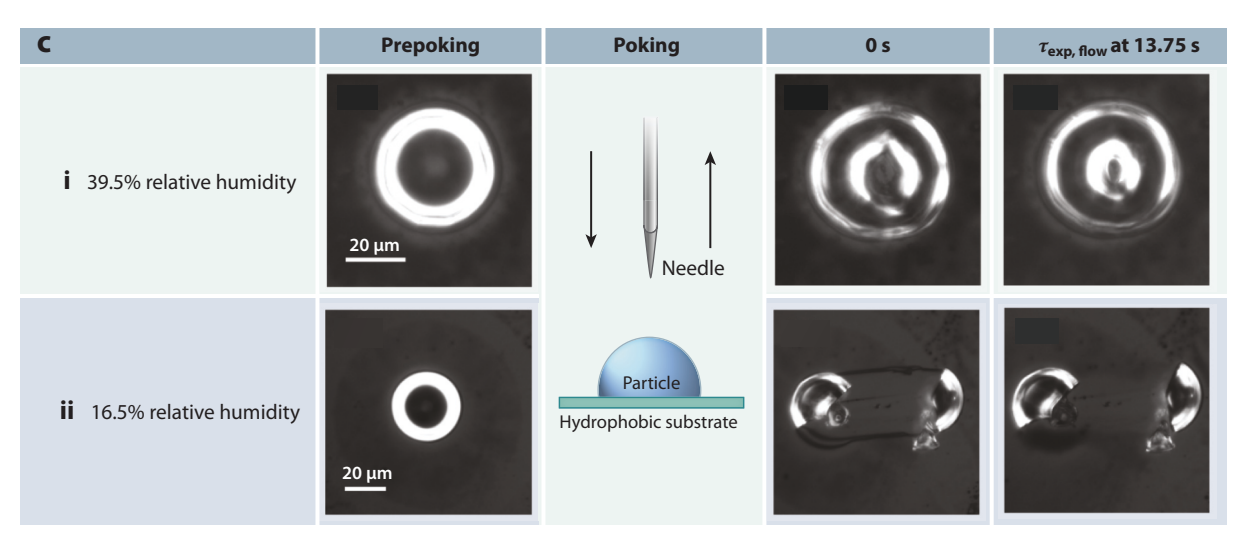


Figure 2

(a) Micrographs of toluene-derived secondary organic material particles with beads. The blue, yellow, and red numbers refer to the x and y coordinates of the beads. (b) Images showing NaCl and sodium dodecyl sulfate coalescence in optical tweezers. a_v/a_v measurements refer to the droplet aspect ratios. Panel b adapted with permission from Reference 69; copyright 2016 Royal Society of Chemistry. (c) Micrographs of toluene-derived secondary organic material before and after poking. Panels a and c adapted with permission from Reference 68 (CC BY 3.0).

> the single-particle force plot data at each RH are analyzed for two parameters: relative indentation depth (RID) and viscoelastic response distance (VRD). The VRD is a measure of the hysteresis in the distance from approach and retract curves at zero force due to the extent of the viscoelastic response. The RID is a ratio of maximum indentation (I) determined from the force plot data at a specified force divided by the height of the particle (H) obtained from the AFM height imaging:

$$RID = \frac{I}{H}.$$
 3.

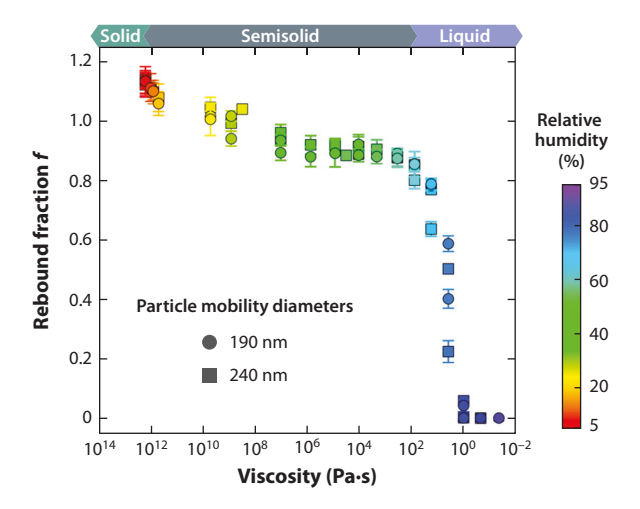


Figure 3

Graph showing the measured particle rebound fraction of submicrometer sucrose particles with varying relative humidities and viscosities. Figure adapted with permission from Reference 72; copyright 2015

American Chemical Society.

If the RID value is close to zero, then the indentation is insignificant compared to the height of the particle (**Figure 4a**), which is indicative of a solid-like particle. If the RID value is approaching one, then the AFM probe pushed completely through the particle, indicative of a liquid-like particle (**Figure 4c**). Previously, the methodology was established to determine solid, semisolid, and liquid phases by testing submicrometer-sized individual sucrose and raffinose particles at varying RHs (42, 44). Here, an RID value equal to or greater than 0.95 was indicative of a liquid, and a value less than 0.95 was indicative of either a solid or a semisolid phase. To distinguish the solid from the semisolid phase (**Figure 4b**), the VRD measurement is assessed. Here, a VRD value greater than 0.5 nm was indicative of a semisolid and less than 0.5 nm was indicative of a solid phase. From these results, a step-by-step framework was developed for identifying the phase state of

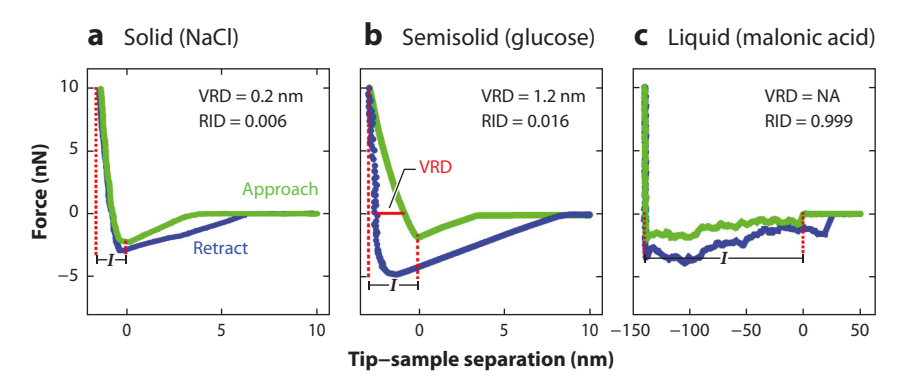


Figure 4

Illustrative atomic force microscopy plots collected on (a) individual solid NaCl, (b) semisolid glucose, and (c) liquid malonic acid particles. VRD and RID measurements are provided and illustrated; I indicates indentation depth. Abbreviations: NA, not applicable; RID, relative indentation depth; VRD, viscoelastic response distance. Figure adapted with permission from Reference 42; copyright 2019 American Chemical Society.

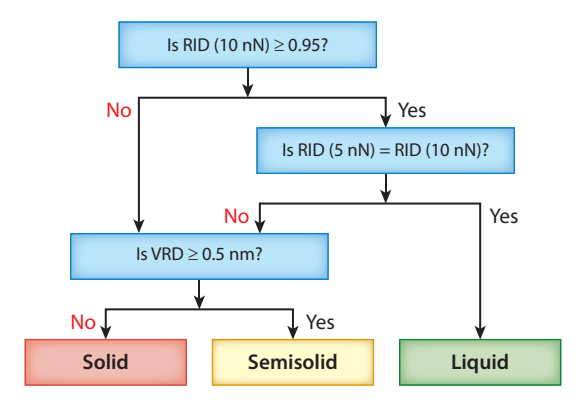


Figure 5

Framework used to identify the phase state of substrate-deposited aerosol particles with atomic force microscopy. If the 10-nN RID value is greater than 0.95 and the difference between that RID value and the 5-nN value is less than 2%, then the difference is treated as statistically insignificant. Abbreviations: RID, relative indentation depth; VRD, viscoelastic response distance. Figure adapted with permission from Reference 42; copyright 2019 American Chemical Society.

individual particles (**Figure 5**). While this approach requires direct contact between the AFM tip and particle, it is an accurate way of identifying the phase state from 10^{-3} to 10^{16} Pa·s in viscosity.

Another AFM method that can assess the phase state for a large number of substrate-deposited particles is based on AFM height imaging (42). Previously, scanning electron microscopy-based shape analysis was used to identify the phase state of substrate-deposited particles (79, 80). Similarly, the aspect ratio of substrate-deposited SSA-relevant particles, which is defined as the particle height divided by the corresponding area equivalent diameter, has been shown to correlate with the phase state of particles from 0.5 to 1.0 µm in size (**Figure 6**). The single-particle aspect ratio can be directly measured from the AFM height image data. From a study of a variety of different SSA-relevant systems, the higher aspect ratio was correlated with a solid-like phase state, whereas the lower aspect ratio was correlated with a liquid-like phase state (42). Specifically, particles with aspect ratios of less than 0.165 were liquid, those between 0.165 and 0.365 were semisolid, and those greater than 0.365 were solid. Additional factors such as the impaction method, the substrate used for impaction, and significantly smaller particles need to be explored to further validate the correlation between the phase state and aspect ratio. However, this methodology proves to be a quick (albeit less accurate than force spectroscopy) technique that is applicable for other microscopy techniques that can quantify the aspect ratio of substrate-deposited particles.

4. SURFACE TENSION MEASUREMENTS OF AEROSOLS

The surface tension of bulk liquids is typically measured using tensiometers. Force tensiometers probe the liquid using a macro-sized needle, typically millimeters in size, forming a meniscus between the needle and liquid (43, 81–83). The force measured to break the meniscus is correlated to the surface tension (84, 85). In contrast, optical tensiometers use a high-resolution charge-coupled device camera to image the shape of the liquid as it is expelled at the end of a needle. The droplet shape factor, along with the known density of the liquid, is required to infer the surface tension by fitting to the Young-Laplace equation (86). Both methodologies are well established, inexpensive, and fast. However, neither can study submicrometer-sized aerosols. The force tensiometer also requires milliliters of sample volume. These inherent size and volume limitations

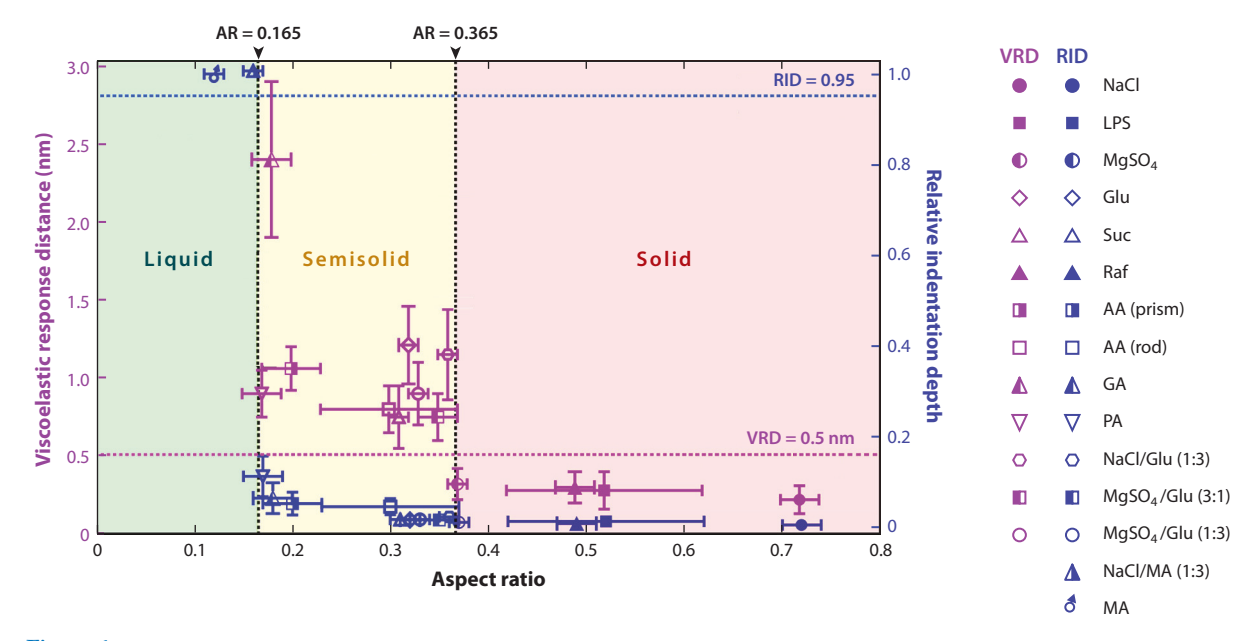


Figure 6

Measured VRD and RID from AFM versus AR measured from AFM height imaging of single and binary chemical systems. Abbreviations: AA, azelaic acid; AFM, atomic force microscopy; AR, aspect ratio; GA, glutaric acid; Glu, glucose; LPS, lipopolysaccharide; MA, malonic acid; PA, palmitic acid; Raf, raffinose; RID, relative indentation depth; Suc, sucrose; VRD, viscoelastic response distance. Figure adapted with permission from Reference 42; copyright 2019 American Chemical Society.

mean that these methods cannot be directly used to measure the surface tension of individual subor supermicrometer aerosols.

As with measurements of hygroscopicity and phase state, AFM has been used to quantify the surface tension of individual submicrometer aerosols in a liquid phase state (43, 45, 46). The methodology uses a constant radius nanoneedle, typically 50–200 nm in diameter, as the AFM probe to both image the particle and measure its surface tension at a variable RH. The latter is illustrated in **Figure 7**. The maximum absolute force required to break the meniscus between the particle and nanoneedle is called the retention force (45) and corresponds to the contact angle approaching zero. By quantifying the retention force measured from indenting into the particle with the nanoneedle at a specific RH, the surface tension can be quantified with the expression (87)

$$F_{\rm ret} = 2\pi r \sigma, 4.$$

where F_{ret} is retention force, r is the radius of the nanoneedle, and σ is the surface tension of the liquid particle. Note that this method is similar to force tensiometers except for the needle size.

This methodology was previously developed in 2015 on SSA-relevant systems (45) and further validated in 2017 on a variety of model systems (43) that included surface-inactive and surface-active chemical systems such as inorganic salts, carboxylic acids, and saccharides (**Figure 8**). In this case, the single-particle AFM surface tension data on particles approximately 500 nm in size correlated well with bulk studies (43). In 2020, this methodology was also successfully applied to quantify the surface tension of real SSAs (**Figure 9**). SSAs produced by the breaking of waves of isolated seawater from California were collected for AFM studies (46). The data revealed a significant particle-to-particle variability that was beyond the analytical uncertainty of the methodology.

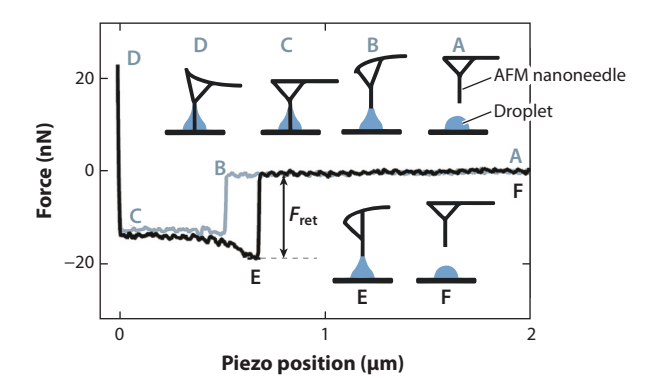


Figure 7

An illustrative force plot for a liquid particle using the atomic force microscopy (AFM) surface tension measurement methodology; retention force ($F_{\rm ret}$) is illustrated. The gray line refers to the approach trace and the black line refers to the retract trace. After imaging the particle, the nanoneedle is positioned above the approximate center of the particle in position A. Then the nanoneedle is lowered at constant speed until it contacts the particle surface in position B and pushes through the particle until it reaches position C. Afterward, the nanoneedle starts to push on the solid substrate below the particle, and it is further pressed until a predefined maximum force is reached at position D. Upon reaching this force, the nanoneedle is retracted until the meniscus between it and the liquid particle breaks in position E. The nanoneedle then is returned to its original position in position F. Figure adapted with permission from Reference 45; copyright 2015 Royal Society of Chemistry.

Furthermore, a statistically significant depression of the average SSA surface tension was observed that corresponded to the highest amount of biological activity in the seawater.

One advantage of AFM is that the surface tension measurement methodology can be used to quantify the surface tension of submicrometer-sized particles at viscosity values of less than 10^2 Pa·s, or when the RID is close to or equal to one. In addition, it is considered to be a direct measurement that does not require additional assumptions to measure the surface tension as a function of RH. However, such direct measurement can also be disadvantageous. As the nanoneedle must come into direct contact with the particle, the nanoneedle may become coated with various organic or inorganic species over multiple uses or may change shape due to repeated force measurements. Thus, the methodology requires careful nanoneedle calibration before and after each experiment using a liquid with known surface tension (e.g., vacuum oil or ultrapure water) (43).

Techniques such as microfluidics or optical tweezers do not require such direct contact. Microfluidics can be used to measure the interfacial tension of droplets under biphasic flow. The droplet deformation as a result of induced flow within the system corresponds to the interfacial tension, which can be measured on supermicrometer-sized droplets (75, 88). Optical tweezers manipulate two suspended aerosols and coalesce them to form oscillating droplets. The surface tension can then be quantified by measuring the backscattering intensity with respect to time when the viscosity is equal to or less than 10^{-3} Pa·s and then performing a fast Fourier transformation (69). When the viscosity is greater than 10^{-3} Pa·s, viscous damping phenomena must be considered. This methodology has been validated on multiple model systems, including salts and surface-active organic acids (**Figure 10**). The data showed good agreement with bulk measurements and predictions from the extended aerosol inorganics model (E-AIM). One advantage of this technique is that the trapped aerosols can be maintained for a long time, enabling

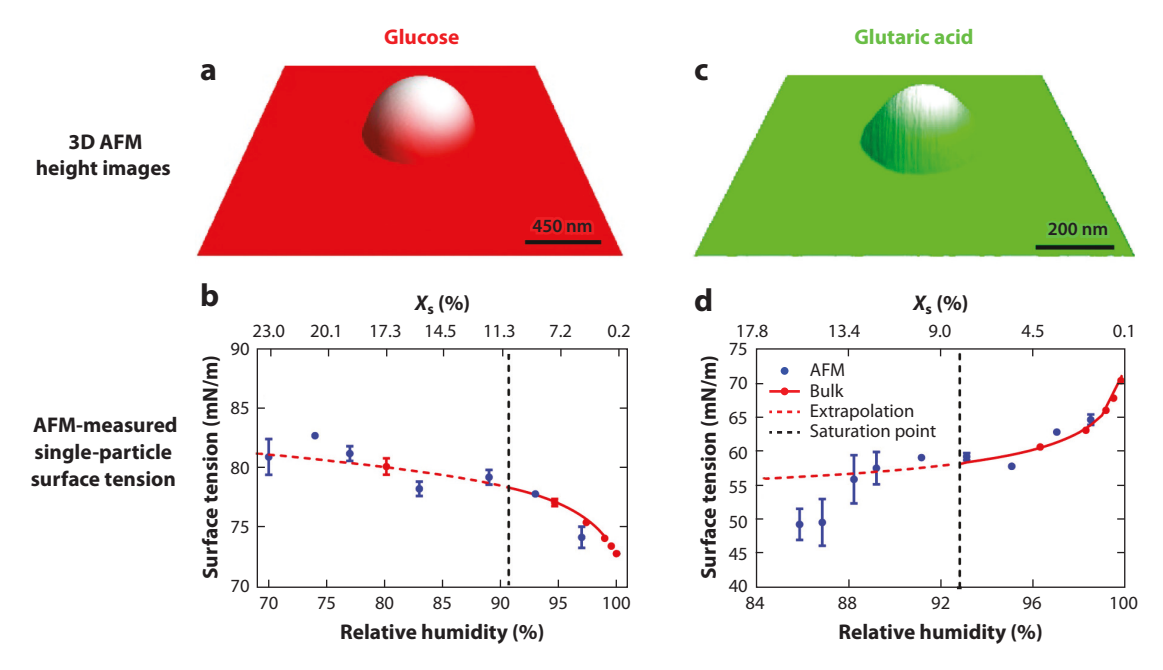


Figure 8

(a,c) Three-dimensional atomic force microscopy (AFM) height images of individual glucose and glutaric acid particles. (b,d) Graphs showing AFM-measured single-particle surface tension versus relative humidity and solute mole percentage for glucose and glutaric acid. Comparisons are made against bulk force tensiometer measurements that have been extrapolated beyond the saturation point. Figure adapted with permission from Reference 43; copyright 2017 American Chemical Society.

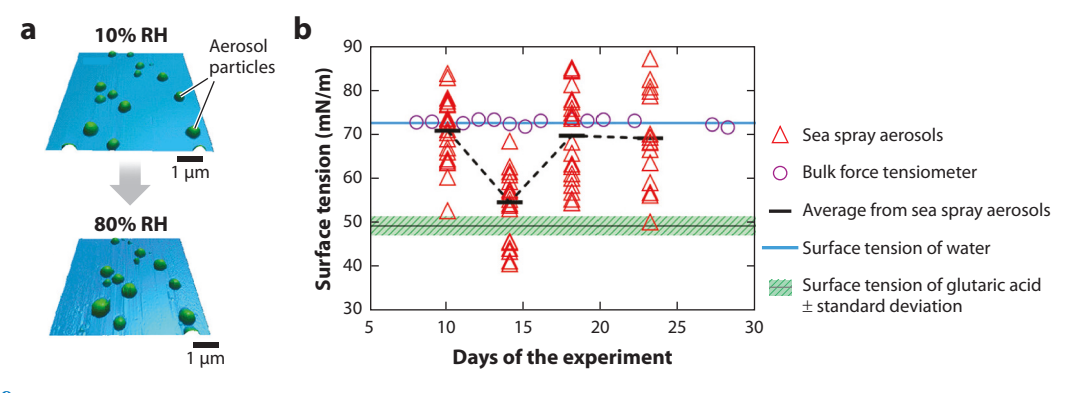
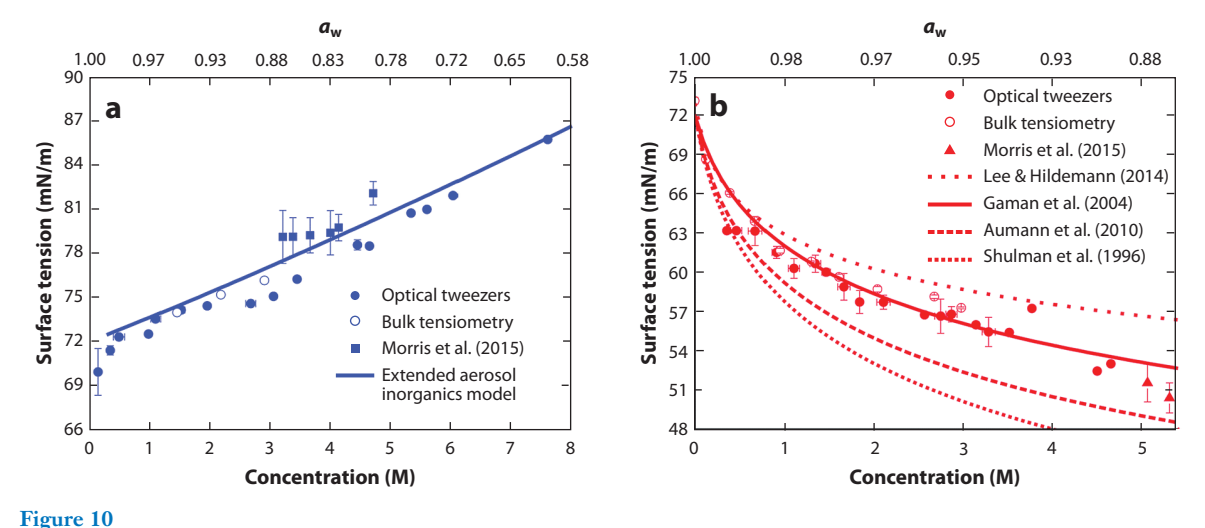


Figure 9

(a) Three-dimensional atomic force microscopy (AFM) height images of (top) individual nascent sea spray aerosol particles at 10% relative humidity (RH) and (bottom) corresponding deliquesced liquid droplets at 80% RH. (b) Graph showing AFM-measured surface tension at 80% RH of individual nascent sea spray aerosols (red open triangles). The averages per day are shown by black horizontal solid lines, which are connected by black dashed lines for illustrative purposes. The surface tension measurement of the seawater with a bulk force tensiometer is shown (purple open circles) as well as the surface tension of water at room temperature (blue solid line). For comparison, the surface tension of glutaric acid measured with AFM at 86% RH, along with the standard deviation, is shown (gray solid line with green diagonal dasbes). Figure adapted with permission from Reference 46; copyright 2020 American Chemical Society.



Graphs of measured surface tension versus concentration and water activity for (a) NaCl and (b) glutaric acid with optical tweezers. Figure adapted with permission from Reference 69; copyright 2016 Royal Society of Chemistry.

controlled time-dependent studies. Furthermore, indirect measurement may be less susceptible to contamination. However, the methodology cannot be applied to submicrometer-sized aerosols. In addition, the surface tension measurements are constrained to viscosities equal to or less than $10^{-2} \text{ Pa} \cdot \text{s}$ (69).

5. CONCLUSION AND FUTURE OUTLOOK

With the emerging role of AFM in studying the physicochemical properties of atmospheric aerosol particles, this review has sought to evaluate how the tool enables, as a function of RH, measurements of the hygroscopicity, phase state, and surface tension of individual substrate-deposited aerosols without prior knowledge of their chemical identity. While the single-particle method does require a substrate and detailed quantification can be time-consuming if a significant number of particles or samples need to be studied, it is applicable for both sub- and supermicrometer-sized aerosols over the range of 10^{-3} – 10^{16} Pa·s in viscosity.

Future studies could build upon the existing work in several ways. First is the extension of the development and validation of hygroscopicity, phase state, and surface tension methodology by applying it toward increasingly more complex model systems (e.g., with a larger number of components and with various mixing states and morphologies) and to varying particle sizes (e.g., below 100 nm). As most of the SSA-relevant systems studied thus far were single-component or binary mixtures approximately 0.5–1.0 µm in size, these are neither complex nor small enough to fully replicate the entire population of real SSAs or other atmospherically relevant particulate matter such as secondary marine aerosols (89–91). To enable surface tension measurements of smaller particles, the development of smaller constant diameter AFM nanoneedles (i.e., less than 50 nm) is required.

Second is the extension of the applicability of the AFM instrumentation used to perform these experiments by changing temperature and/or introducing heterogeneous gases in situ to better simulate the atmospheric conditions. While AFM allows the RH to be readily controlled, current technological limitations prevent successful force spectroscopy experiments that can lower

the temperature to and maintain it below -38° C for AFM experiments under ambient pressure. The capability to reach and maintain such low temperatures will be important in replicating the atmospheric conditions relevant for ice nucleation studies (11, 52). Introducing the gases commonly found in the atmosphere (92) to the substrate-deposited particles in situ during AFM force spectroscopy and imaging experiments may yield insights into the heterogeneous chemistry and atmospheric aging dynamics of aerosols.

Third is the development of the methodology to quantify the viscosity of an individual particle at varying RHs. While the AFM phase state methodology is broadly applicable at low to high RHs, each system exhibits a wide range of viscosities within a specific phase state. In the future, AFM must be able to quantify the viscosity in addition to probing the phase state of submicrometer-sized aerosols.

Lastly is the incorporation of new innovations into AFM technology. New developments such as the amplitude and frequency modulation technique hold promise to both image and map certain physicochemical properties of individual aerosols, such as the Young's modulus and the viscosity coefficient (93–95). This has the potential to allow facile imaging and quantification of the viscosity and phase state on a single-particle basis with the desired spatial resolution (e.g., nanometer level) as a function of RH. Such development could allow for a significant increase in the number of individual aerosols characterized, thus enabling much larger populations of particles to be studied. Also, the relatively recent development of AFM-infrared photothermal spectroscopy allows for both AFM imaging and the spectroscopic characterization of aerosols (6, 96). Using AFM methodology concurrently with chemical imaging may enable direct correspondence between the chemical composition and property of the aerosol. Such measurements on real aerosols may lead to new insights and improved understanding of the roles of aerosols on the climate, atmosphere, and human health.

DISCLOSURE STATEMENT

The authors are not aware of any affiliations, memberships, funding, or financial holdings that might be perceived as affecting the objectivity of this review.

ACKNOWLEDGMENTS

This work was funded by the National Science Foundation (NSF) through the NSF Center for Aerosol Impacts on Chemistry of the Environment (CAICE) under grant CHE-1801971. The authors would like to thank Jonathan H. Slade, Cari S. Dutcher, Paul (Ryan) Tumminello, and Priyatanu Roy for helpful discussions.

LITERATURE CITED

- Pöschl U. 2005. Atmospheric aerosols: composition, transformation, climate and health effects. Angew. Chem. Int. Ed. 44:7520–40
- Riemer N, Ault AP, West M, Craig RL, Curtis JH. 2019. Aerosol mixing state: measurements, modeling, and impacts. Rev. Geophys. 57:187–249
- Wang XF, Deane GB, Moore KA, Ryder OS, Stokes MD, et al. 2017. The role of jet and film drops in controlling the mixing state of submicron sea spray aerosol particles. PNAS 114:6978–83
- Cochran RE, Laskina O, Trueblood JV, Estillore AD, Morris HS, et al. 2017. Molecular diversity of sea spray aerosol particles: impact of ocean biology on particle composition and hygroscopicity. Chem 2:655–67

- Zhang Y, Chen Y, Lambe AT, Olson NE, Lei Z, et al. 2018. Effect of the aerosol-phase state on secondary
 organic aerosol formation from the reactive uptake of isoprene-derived epoxydiols (IEPOX). Environ.
 Sci. Technol. Lett. 5:167–74
- Bondy AL, Kirpes RM, Merzel RL, Pratt KA, Banaszak Holl MM, Ault AP. 2017. Atomic force microscopy-infrared spectroscopy of individual atmospheric aerosol particles: subdiffraction limit vibrational spectroscopy and morphological analysis. *Anal. Chem.* 89:8594–98
- Shiraiwa M, Ueda K, Pozzer A, Lammel G, Kampf CJ, et al. 2017. Aerosol health effects from molecular to global scales. Environ. Sci. Technol. 51:13545–67
- Haywood J, Boucher O. 2000. Estimates of the direct and indirect radiative forcing due to tropospheric aerosols: a review. Rev. Geophys. 38:513–43
- Seinfeld JH, Bretherton C, Carslaw KS, Coe H, DeMott PJ, et al. 2016. Improving our fundamental understanding of the role of aerosol-cloud interactions in the climate system. PNAS 113:5781–90
- Petters MD, Kreidenweis SM. 2007. A single parameter representation of hygroscopic growth and cloud condensation nucleus activity. Atmos. Chem. Phys. 7:1961–71
- McCluskey CS, Hill TCJ, Malfatti F, Sultana CM, Lee C, et al. 2017. A dynamic link between ice nucleating particles released in nascent sea spray aerosol and oceanic biological activity during two mesocosm experiments. *7. Atmos. Sci.* 74:151–66
- IPCC (Intergov. Panel Clim. Chang.). 2013. Climate Change 2013: The Physical Science Basis. Contribution of Working Group I to the Fifth Assessment Report of the Intergovernmental Panel on Climate Change. Cambridge, UK/New York: Cambridge Univ. Press
- Hodas N, Zuend A, Mui W, Flagan RC, Seinfeld JH. 2015. Influence of particle-phase state on the hygroscopic behavior of mixed organic-inorganic aerosols. Atmos. Chem. Phys. 15:5027–45
- Schill SR, Collins DB, Lee C, Morris HS, Novak GA, et al. 2015. The impact of aerosol particle mixing state on the hygroscopicity of sea spray aerosol. ACS Central Sci. 1:132–41
- Berkemeier T, Shiraiwa M, Pöschl U, Koop T. 2014. Competition between water uptake and ice nucleation by glassy organic aerosol particles. Atmos. Chem. Phys. 14:12513–31
- Collins DB, Ault AP, Moffet RC, Ruppel MJ, Cuadra-Rodriguez LA, et al. 2013. Impact of marine biogeochemistry on the chemical mixing state and cloud forming ability of nascent sea spray aerosol. J. Geophys. Res. Atmos. 118:8553–65
- Stock M, Cheng YF, Birmili W, Massling A, Wehner B, et al. 2011. Hygroscopic properties of atmospheric aerosol particles over the Eastern Mediterranean: implications for regional direct radiative forcing under clean and polluted conditions. Atmos. Chem. Phys. 11:4251–71
- Tandon A, Rothfuss NE, Petters MD. 2019. The effect of hydrophobic glassy organic material on the cloud condensation nuclei activity of particles with different morphologies. *Atmos. Chem. Phys.* 19:3325– 39
- Shiraiwa M, Li Y, Tsimpidi AP, Karydis VA, Berkemeier T, et al. 2017. Global distribution of particle phase state in atmospheric secondary organic aerosols. *Nat. Commun.* 8:15002
- Shiraiwa M, Zuend A, Bertram AK, Seinfeld JH. 2013. Gas-particle partitioning of atmospheric aerosols: interplay of physical state, non-ideal mixing and morphology. Phys. Chem. Chem. Phys. 15:11441–53
- Renbaum-Wolff L, Grayson JW, Bateman AP, Kuwata M, Sellier M, et al. 2013. Viscosity of α-pinene secondary organic material and implications for particle growth and reactivity. PNAS 110:8014–19
- Kuwata M, Martin ST. 2012. Phase of atmospheric secondary organic material affects its reactivity. PNAS 109:17354–59
- Saukko E, Lambe AT, Massoli P, Koop T, Wright JP, et al. 2012. Humidity-dependent phase state of SOA particles from biogenic and anthropogenic precursors. Atmos. Chem. Phys. 12:7517–29
- Shiraiwa M, Ammann M, Koop T, Pöschl U. 2011. Gas uptake and chemical aging of semisolid organic aerosol particles. PNAS 108:11003–8
- Virtanen A, Joutsensaari J, Koop T, Kannosto J, Yli-Pirila P, et al. 2010. An amorphous solid state of biogenic secondary organic aerosol particles. *Nature* 467:824–27
- Zobrist B, Marcolli C, Pedernera DA, Koop T. 2008. Do atmospheric aerosols form glasses? Atmos. Chem. Phys. 8:5221–44
- Davies JF, Zuend A, Wilson KR. 2019. Technical note: the role of evolving surface tension in the formation of cloud droplets. Atmos. Chem. Phys. 19:2933–46

- Forestieri SD, Staudt SM, Kuborn TM, Faber K, Ruehl CR, et al. 2018. Establishing the impact of model surfactants on cloud condensation nuclei activity of sea spray aerosol mimics. Atmos. Chem. Phys. 18:10985–1005
- Ovadnevaite J, Zuend A, Laaksonen A, Sanchez KJ, Roberts G, et al. 2017. Surface tension prevails over solute effect in organic-influenced cloud droplet activation. *Nature* 546:637–41
- Ruehl CR, Davies JF, Wilson KR. 2016. An interfacial mechanism for cloud droplet formation on organic aerosols. Science 351:1447–50
- Facchini MC, Mircea M, Fuzzi S, Charlson RJ. 1999. Cloud albedo enhancement by surface-active organic solutes in growing droplets. *Nature* 401:257–59
- 32. Giessibl FJ. 2003. Advances in atomic force microscopy. Rev. Mod. Phys. 75:949-83
- Ault AP, Axson JL. 2017. Atmospheric aerosol chemistry: spectroscopic and microscopic advances. Anal. Chem. 89:430–52
- Gan Y. 2009. Atomic and subnanometer resolution in ambient conditions by atomic force microscopy. Surf. Sci. Rep. 64:99–121
- Lansakara TI, Morris HS, Singh P, Kohen A, Tivanski AV. 2020. Rigid double-stranded DNA linkers for single molecule enzyme–drug interaction measurements using molecular recognition force spectroscopy. *Langmuir* 36:4174–83
- Poggi MA, Gadsby ED, Bottomley LA, King WP, Oroudjev E, Hansma H. 2004. Scanning probe microscopy. Anal. Chem. 76:3429–44
- Martínez NF, Lozano JR, Herruzo ET, Garcia F, Richter C, et al. 2008. Bimodal atomic force microscopy imaging of isolated antibodies in air and liquids. Nanotechnology 19:384011
- Martínez NF, García R. 2006. Measuring phase shifts and energy dissipation with amplitude modulation atomic force microscopy. Nanotechnology 17:S167–72
- Scott WW, Bhushan B. 2003. Use of phase imaging in atomic force microscopy for measurement of viscoelastic contrast in polymer nanocomposites and molecularly thick lubricant films. *Ultramicroscopy* 97:151–69
- Nagao E, Dvorak JA. 1999. Phase imaging by atomic force microscopy: analysis of living homoiothermic vertebrate cells. *Biophys.* 7, 76:3289–97
- Bar G, Thomann Y, Brandsch R, Cantow H-J, Whangbo M-H. 1997. Factors affecting the height and phase images in tapping mode atomic force microscopy. Study of phase-separated polymer blends of poly(ethene-co-styrene) and poly(2,6-dimethyl-1,4-phenylene oxide). *Langmuir* 13:3807–12
- Ray KK, Lee HD, Gutierrez MA, Chang FJ, Tivanski AV. 2019. Correlating 3D morphology, phase state, and viscoelastic properties of individual substrate-deposited particles. *Anal. Chem.* 91:7621–30
- Lee HD, Estillore AD, Morris HS, Ray KK, Alejandro A, et al. 2017. Direct surface tension measurements of individual sub-micrometer particles using atomic force microscopy. J. Phys. Chem. A 121:8296

 305
- Lee HD, Ray KK, Tivanski AV. 2017. Solid, semisolid, and liquid phase states of individual submicrometer particles directly probed using atomic force microscopy. *Anal. Chem.* 89:12720–26
- Morris HS, Grassian VH, Tivanski AV. 2015. Humidity-dependent surface tension measurements of individual inorganic and organic submicrometre liquid particles. Chem. Sci. 6:3242–47
- Lee HD, Morris HS, Laskina O, Sultana CM, Lee C, et al. 2020. Organic enrichment, physical phase state, and surface tension depression of nascent core–shell sea spray aerosols during two phytoplankton blooms. ACS Earth Space Chem. 4:650–60
- Laskina O, Morris HS, Grandquist JR, Qiu Z, Stone EA, et al. 2015. Size matters in the water uptake and hygroscopic growth of atmospherically relevant multicomponent aerosol particles. J. Phys. Chem. A 119:4489–97
- Estillore AD, Morris HS, Or VW, Lee HD, Alves MR, et al. 2017. Linking hygroscopicity and the surface microstructure of model inorganic salts, simple and complex carbohydrates, and authentic sea spray aerosol particles. *Phys. Chem. Chem. Phys.* 19:21101–11
- Morris HS, Estillore AD, Laskina O, Grassian VH, Tivanski AV. 2016. Quantifying the hygroscopic growth of individual submicrometer particles with atomic force microscopy. *Anal. Chem.* 88:3647–54
- Lee HD, Kaluarachchi CP, Hasenecz ES, Zhu JZ, Popa E, et al. 2019. Effect of dry or wet substrate deposition on the organic volume fraction of core–shell aerosol particles. Atmos. Meas. Tech. 12:2033–42

- Laskina O, Morris HS, Grandquist JR, Estillore AD, Stone EA, et al. 2015. Substrate-deposited sea spray aerosol particles: influence of analytical method, substrate, and storage conditions on particle size, phase, and morphology. *Environ. Sci. Technol.* 49:13447–53
- 52. DeMott PJ, Hill TCJ, McCluskey CS, Prather KA, Collins DB, et al. 2016. Sea spray aerosol as a unique source of ice nucleating particles. *PNAS* 113:5797–803
- DeMott PJ, Prenni AJ, Liu X, Kreidenweis SM, Petters MD, et al. 2010. Predicting global atmospheric ice nuclei distributions and their impacts on climate. PNAS 107:11217–22
- Jayarathne T, Sultana CM, Lee C, Malfatti F, Cox JL, et al. 2016. Enrichment of saccharides and divalent cations in sea spray aerosol during two phytoplankton blooms. *Environ. Sci. Technol.* 50:11511–20
- Dutcher CS, Ge XL, Wexler AS, Clegg SL. 2013. An isotherm-based thermodynamic model of multicomponent aqueous solutions, applicable over the entire concentration range. J. Phys. Chem. A 117:3198– 213
- Marshall FH, Miles REH, Song YC, Ohm PB, Power RM, et al. 2016. Diffusion and reactivity in ultraviscous aerosol and the correlation with particle viscosity. Chem. Sci. 7:1298–308
- Song YC, Haddrell AE, Bzdek BR, Reid JP, Barman T, et al. 2016. Measurements and predictions of binary component aerosol particle viscosity. 7. Phys. Chem. A 120:8123–37
- Murray BJ, Wilson TW, Dobbie S, Cui ZQ, Al-Jumur SMRK, et al. 2010. Heterogeneous nucleation of ice particles on glassy aerosols under cirrus conditions. Nat. Geosci. 3:233–37
- Baustian KJ, Wise ME, Jensen EJ, Schill GP, Freedman MA, Tolbert MA. 2013. State transformations and ice nucleation in amorphous (semi-)solid organic aerosol. Atmos. Chem. Phys. 13:5615–28
- Murray BJ. 2008. Inhibition of ice crystallisation in highly viscous aqueous organic acid droplets. Atmos. Chem. Phys. 8:5423–33
- Mikhailov E, Vlasenko S, Martin ST, Koop T, Poeschl U. 2009. Amorphous and crystalline aerosol particles interacting with water vapor: conceptual framework and experimental evidence for restructuring, phase transitions and kinetic limitations. Atmos. Chem. Phys. 9:9491–522
- Pilinis C, Pandis SN, Seinfeld JH. 1995. Sensitivity of direct climate forcing by atmospheric aerosols to aerosol size and composition. J. Geophys. Res. Atmos. 100:18739–54
- Ruehl CR, Wilson KR. 2014. Surface organic mono layers control the hygroscopic growth of submicrometer particles at high relative humidity. J. Phys. Chem. A 118:3952–66
- Ruehl CR, Chuang PY, Nenes A. 2010. Aerosol hygroscopicity at high (99 to 100%) relative humidities. *Atmos. Chem. Phys.* 10:1329–44
- 65. Barnes HA, Hutton JF, Walters K. 1989. An Introduction to Rheology. Amsterdam: Elsevier
- Reid JP, Bertram AK, Topping DO, Laskin A, Martin ST, et al. 2018. The viscosity of atmospherically relevant organic particles. Nat. Commun. 9:956
- Renbaum-Wolff L, Grayson JW, Bertram AK. 2013. Technical note: new methodology for measuring viscosities in small volumes characteristic of environmental chamber particle samples. Atmos. Chem. Phys. 13:791–802
- Song MJ, Liu PFF, Hanna SJ, Zaveri RA, Potter K, et al. 2016. Relative humidity-dependent viscosity of secondary organic material from toluene photo-oxidation and possible implications for organic particulate matter over megacities. *Atmos. Chem. Phys.* 16:8817–30
- Bzdek BR, Power RM, Simpson SH, Reid JP, Royall CP. 2016. Precise, contactless measurements of the surface tension of picolitre aerosol droplets. Chem. Sci. 7:274

 –85
- Power RM, Simpson SH, Reid JP, Hudson AJ. 2013. The transition from liquid to solid-like behaviour in ultrahigh viscosity aerosol particles. Chem. Sci. 4:2597–604
- Grayson JW, Song M, Sellier M, Bertram AK. 2015. Validation of the poke-flow technique combined with simulations of fluid flow for determining viscosities in samples with small volumes and high viscosities. Atmos. Meas. Tech. 8:2463–72
- Bateman AP, Bertram AK, Martin ST. 2015. Hygroscopic influence on the semisolid-to-liquid transition of secondary organic materials. J. Phys. Chem. A 119:4386–95
- Bateman AP, Belassein H, Martin ST. 2014. Impactor apparatus for the study of particle rebound: relative humidity and capillary forces. Aerosol Sci. Technol. 48:42–52

- Slade JH, Ault AP, Bui AT, Ditto JC, Lei Z, et al. 2019. Bouncier particles at night: biogenic secondary organic aerosol chemistry and sulfate drive diel variations in the aerosol phase in a mixed forest. *Environ.* Sci. Technol. 53:4977–87
- Roy P, Liu S, Dutcher CS. 2020. Droplet interfacial tensions and phase transitions measured in microfluidic channels. *Annu. Rev. Phys. Chem.* 72:73–98
- Nandy L, Liu S, Gunsbury C, Wang X, Pendergraft MA, et al. 2019. Multistep phase transitions in sea surface microlayer droplets and aerosol mimics using microfluidic wells. ACS Earth Space Chem. 3:1260– 67
- Nandy L, Dutcher CS. 2018. Phase behavior of ammonium sulfate with organic acid solutions in aqueous aerosol mimics using microfluidic traps. J. Phys. Chem. B 122:3480–90
- Metcalf AR, Narayan S, Dutcher CS. 2018. A review of microfluidic concepts and applications for atmospheric aerosol science. Aerosol Sci. Technol. 52:310–29
- Wang B, Harder TH, Kelly ST, Piens DS, China S, et al. 2016. Airborne soil organic particles generated by precipitation. *Nat. Geosci.* 9:433–37
- O'Brien RE, Neu A, Epstein SA, MacMillan AC, Wang B, et al. 2014. Physical properties of ambient and laboratory-generated secondary organic aerosol. Geophys. Res. Lett. 41:4347–53
- 81. Lee JY, Hildemann LM. 2013. Surface tension of solutions containing dicarboxylic acids with ammonium sulfate, p-glucose, or humic acid. 7. Aerosol Sci. 64:94–102
- Lee BB, Chan ES, Ravindra P, Khan TA. 2012. Surface tension of viscous biopolymer solutions measured using the du Nouy ring method and the drop weight methods. *Polymer Bull*. 69:471–89
- Tuckermann R. 2007. Surface tension of aqueous solutions of water-soluble organic and inorganic compounds. Atmos. Environ. 41:6265–75
- 84. Padday JF, Pitt AR, Pashley RM. 1975. Menisci at a free liquid surface: surface tension from the maximum pull on a rod. 7. Chem. Soc. Faraday Trans. 1 Phys. Chem. Condensed Phases 71:1919–31
- Harkins WD, Jordan HF. 1930. A method for the determination of surface and interfacial tension from the maximum pull on a ring. 7. Am. Chem. Soc. 52:1751–72
- Berry JD, Neeson MJ, Dagastine RR, Chan DYC, Tabor RF. 2015. Measurement of surface and interfacial tension using pendant drop tensiometry. J. Colloid Interface Sci. 454:226–37
- Yazdanpanah MM, Hosseini M, Pabba S, Berry SM, Dobrokhotov VV, et al. 2008. Micro-Wilhelmy and related liquid property measurements using constant-diameter nanoneedle-tipped atomic force microscope probes. *Langmuir* 24:13753–64
- Boyer HC, Dutcher CS. 2017. Atmospheric aqueous aerosol surface tensions: isotherm-based modeling and biphasic microfluidic measurements. 7. Phys. Chem. A 121:4733–42
- Bertram TH, Cochran RE, Grassian VH, Stone EA. 2018. Sea spray aerosol chemical composition: elemental and molecular mimics for laboratory studies of heterogeneous and multiphase reactions. *Chem. Soc. Rev.* 47:2374

 –400
- Prather KA, Bertram TH, Grassian VH, Deane GB, Stokes MD, et al. 2013. Bringing the ocean into the laboratory to probe the chemical complexity of sea spray aerosol. PNAS 110:7550–55
- Trueblood JV, Wang X, Or VW, Alves MR, Santander MV, et al. 2019. The old and the new: aging
 of sea spray aerosol and formation of secondary marine aerosol through OH oxidation reactions. ACS
 Earth Space Chem. 3:2307–14
- Estillore AD, Trueblood JV, Grassian VH. 2016. Atmospheric chemistry of bioaerosols: heterogeneous and multiphase reactions with atmospheric oxidants and other trace gases. Chem. Sci. 7:6604–16
- Benaglia S, Gisbert VG, Perrino AP, Amo CA, Garcia R. 2018. Fast and high-resolution mapping of elastic properties of biomolecules and polymers with bimodal AFM. Nat. Protoc. 13:2890–907
- Amo CA, Perrino AP, Payam AF, Garcia R. 2017. Mapping elastic properties of heterogeneous materials in liquid with angstrom-scale resolution. ACS Nano 11:8650–59
- Herruzo ET, Perrino AP, Garcia R. 2014. Fast nanomechanical spectroscopy of soft matter. Nat. Commun. 5:3126
- Or VW, Estillore AD, Tivanski AV, Grassian VH. 2018. Lab on a tip: atomic force microscopy photothermal infrared spectroscopy of atmospherically relevant organic/inorganic aerosol particles in the nanometer to micrometer size range. Analyst 143:2765–74

- Lee JY, Hildemann LM. 2014. Surface tensions of solutions containing dicarboxylic acid mixtures. Atmos. Environ. 89:260–67
- 98. Gaman AI, Kulmala M, Vehkamaki H, Napari I, Mircea M, et al. 2004. Binary homogeneous nucleation in water-succinic acid and water-glutaric acid systems. *7. Chem. Phys.* 120:282–91
- 99. Aumann E, Hildemann LM, Tabazadeh A. 2010. Measuring and modeling the composition and temperature-dependence of surface tension for organic solutions. *Atmos. Environ.* 44:329–37
- Shulman ML, Jacobson MC, Carlson RJ, Synovec RE, Young TE. 1996. Dissolution behavior and surface tension effects of organic compounds in nucleating cloud droplets. *Geophys. Res. Lett.* 23:277–80



Contents

My Trajectory in Molecular Reaction Dynamics and Spectroscopy **Robert Benny Gerber**	. 1
My Life in Changing Times: New Ideas and New Techniques *Ruth M. Lynden-Bell	3 5
Critical Phenomena in Plasma Membrane Organization and Function Thomas R. Shaw, Subhadip Ghosh, and Sarah L. Veatch	51
Droplet Interfacial Tensions and Phase Transitions Measured in Microfluidic Channels Priyatanu Roy, Shihao Liu, and Cari S. Dutcher	73
First-Principles Insights into Plasmon-Induced Catalysis John Mark P. Martirez, Junwei Lucas Bao, and Emily A. Carter	99
Optical Properties and Excited-State Dynamics of Atomically Precise Gold Nanoclusters Meng Zhou and Rongchao Jin	21
α-Crystallins in the Vertebrate Eye Lens: Complex Oligomers and Molecular Chaperones Marc A. Sprague-Piercy, Megan A. Rocha, Ashley O. Kwok, and Rachel W. Martin 14	43
Vibronic and Environmental Effects in Simulations of Optical Spectroscopy Tim J. Zuehlsdorff, Sapana V. Shedge, Shao-Yu Lu, Hanbo Hong, Vincent P. Aguirre, Liang Shi, and Christine M. Isborn	65
Molecular Simulation of Electrode-Solution Interfaces Laura Scalfi, Mathieu Salanne, and Benjamin Rotenberg	39
Electrochemical Tip-Enhanced Raman Spectroscopy: An In Situ Nanospectroscopy for Electrochemistry Sheng-Chao Huang, Yi-Fan Bao, Si-Si Wu, Teng-Xiang Huang, Matthew M. Sartin, Xiang Wang, and Bin Ren	13

Atomic Force Microscopy: An Emerging Tool in Measuring the Phase State and Surface Tension of Individual Aerosol Particles Hansol D. Lee and Alexei V. Tivanski	235
Cryogenic Super-Resolution Fluorescence and Electron Microscopy Correlated at the Nanoscale Peter D. Dahlberg and W. E. Moerner	253
Vibrational Sum-Frequency Generation Hyperspectral Microscopy for Molecular Self-Assembled Systems Haoyuan Wang and Wei Xiong	279
Quantitative Mass Spectrometry Imaging of Biological Systems Daisy Unsihuay, Daniela Mesa Sanchez, and Julia Laskin	307
In Situ Surface-Enhanced Raman Spectroscopy Characterization of Electrocatalysis with Different Nanostructures Bao-Ying Wen, Qing-Qi Chen, Petar M. Radjenovic, Jin-Chao Dong, Zhong-Qun Tian, and Jian-Feng Li	331
Quantum-State Control and Manipulation of Paramagnetic Molecules with Magnetic Fields Brianna R. Heazlewood	353
Dry Deposition of Atmospheric Aerosols: Approaches, Observations, and Mechanisms Delphine K. Farmer, Erin K. Boedicker, and Holly M. DeBolt	375
Spectroscopy and Scattering Studies Using Interpolated Ab Initio Potentials Ernesto Quintas-Sánchez and Richard Dawes	399
Control of Chemical Reaction Pathways by Light–Matter Coupling Dinumol Devasia, Ankita Das, Varun Mohan, and Prashant K. Jain	
First-Principles Simulations of Biological Molecules Subjected to Ionizing Radiation Karwan Ali Omar, Karim Hasnaoui, and Aurélien de la Lande	445
Cascaded Biocatalysis and Bioelectrocatalysis: Overview and Recent Advances Yoo Seok Lee, Koun Lim, and Shelley D. Minteer	467
Multiscale Models for Light-Driven Processes Michele Nottoli, Lorenzo Cupellini, Filippo Lipparini, Giovanni Granucci, and Benedetta Mennucci	489
Modeling Spin-Crossover Dynamics Saikat Mukherjee, Dmitry A. Fedorov, and Sergey A. Varganov	515

Multiconfiguration Pair-Density Functional Theory Prachi Sharma, Jie J. Bao, Donald G. Truhlar, and Laura Gagliardi	541
Optical Force-Induced Chemistry at Solution Surfaces Hiroshi Masuhara and Ken-ichi Yuyama	565
Quantum Dynamics of Exciton Transport and Dissociation in Multichromophoric Systems Irene Burghardt, Wjatscheslaw Popp, Dominik Brey, and Robert Binder	591
Understanding and Controlling Intersystem Crossing in Molecules Christel M. Marian	
From Intermolecular Interaction Energies and Observable Shifts to Component Contributions and Back Again: A Tale of Variational Energy Decomposition Analysis Yuezhi Mao, Matthias Loipersberger, Paul R. Horn, Akshaya Kumar Das, Omar Demerdash, Daniel S. Levine, Srimukh Prasad Veccham, Teresa Head-Gordon, and Martin Head-Gordon	641
Demystifying the Diffuse Vibrational Spectrum of Aqueous Protons Through Cold Cluster Spectroscopy Helen J. Zeng and Mark A. Johnson	667

Errata

An online log of corrections to *Annual Review of Physical Chemistry* articles may be found at http://www.annualreviews.org/errata/physchem